Bonding strength calculation in multicomponent plastic processing technologies

Szuchács A., Ageyeva T., Boros R., Kovács J. G.

Accepted for publication in MATERIALS AND MANUFACTURING PROCESSES
Published in 2021
DOI: 10.1080/10426914.2021.1948052

Bonding strength calculation in multicomponent plastic processing technologies

A. Szuchács [a], T. Ageyeva [a, b], R. Boros [a], J. G. Kovács [* a, b]

[a] *Department of Polymer Engineering, Faculty of Mechanical Engineering, Budapest University of Technology and Economics, Műegyetem rkp. 3., H-1111 Budapest, Hungary;*

[b] *MTA-BME Lendület Lightweight Polymer Composites Research Group, Budapest, Hungary*

[*]Corresponding author, e-mail: kovacs@pt.bme.hu

Bonding strength calculation in multicomponent plastic processing technologies

This study focuses on overmolding, a unique injection molding process. It enables a seamless combination of multiple materials into a single part. The bottleneck of overmolding is the interface strength between the paired elements. Interface strength depends on numerous factors, such as the interface topology, the physical and chemical properties of the paired materials, and the processing parameters of overmolding. These factors have a large number of possible combinations. This necessitates a modeling approach to predict the interface properties and find the optimal processing parameters of overmolding at an early design stage. Although injection molding is a well-known field for simulation, adhesion modeling between the substrate and overmolded elements is missing in all available simulation software. Our goal is to develop a simulation methodology that combines analytical models with simulation tools, to predict interface strength during overmolding. The principal novelty of the proposed methodology is that it considers the space-time dependency of the interface temperature—this has a significant influence on interface strength. We proved that the methodology we developed gives the most accurate results; it predicts the bonding strength of overmolded ABS, PC and PS parts with an error of less than 7%.

Keywords: overmolding; bonding; reptation; injection; molding

Introduction

Modern automobile structures have to satisfy several contradictory requirements, such as light weight, high strength and stiffness, low cost, and recyclability. Thermoplastic composite materials (TCMs) seem to be the perfect choice to meet these requirements.[1] However, despite their high potential, TCMs have only had a limited role in the automotive industry as decorative and non-structural elements, until very recently. This has now changed because the latest advances in TCM technologies have brought this class of materials to the forefront. Today, several automated TCM technologies exist. Some of them, such as injection molding, thermoforming and automated tape placement

(ATP) are already widely used in the automotive industry. Others, such as additive manufacturing[2,3] and thermoplastic resin transfer molding (T-RTM), have just started to become popular[4-7].

Although thermoforming and injection molding are usually considered mature technologies with short cycle times (in the range of seconds), the parts produced are limited in geometry and mechanical performance. Therefore, a decade ago, the scientific and industrial community started to develop “hybrid” or “integrated” processes, which are a combination of two TCM technologies (Figure 1)[7-10]. In these hybrid methods, a rigid thermoplastic substrate is produced in the first step, and additional structural elements are built on the surface of the substrate in the second step. The name of the second step depends on the technology used, for example, “overmolding” or “overprinting”. The resulting TCM structures may include stiffness ribs, undercuts, inserts, and other sophisticated features, which improve the performance of the part. At the same time, structures produced via hybrid TCM processing methods can be 20–30% lighter compared to alternatives manufactured by conventional technologies[7,8]. Consequently, hybrid TCM methods are suitable for the production of semi-structural and even structural automotive parts (e.g. floors, door panels, crossbeams, airbag modules, and others).

Despite all their advantages, hybrid TCM processes have drawbacks. Their weak point is the bonding between the coupled elements; bonding strength is usually much weaker than the strength of the material of the individual components. Therefore, one of the challenges is to achieve the level of material strength in the bond.

Bonding between coupled thermoplastic parts in the case of all processing technologies is governed by fusion. It is the result of heat and pressure applied to the interface for a certain amount of time[11-15]. Therefore, the bonding strength (σ) between

thermoplastic parts is generally a function of processing temperature (T), holding pressure (p), and processing time (t):

$$\sigma = f\ (T, p, t).$$

One of the most attractive hybrid TCM processes for automotive applications is the combination of the fastest techniques—thermoforming or injection molding as the first step and injection molding as the second step[16,17]. The bonding strength between the substrate and overmolded elements depends on the processing parameters of injection molding, such as melt and mold temperature (T_{melt} and T_{mold}), holding pressure, and holding time (p_{hold} and t_{hold}). Candal et al.[18] demonstrated that an increase in melt temperature, and in some cases of mold temperature, strengthens the adhesion between a polypropylene (PP) substrate and the overmolded vulcanized thermoplastic elastomer Santoprene. In contrast, the effect of holding pressure and injection rate on bonding strength was almost negligible. Giusti and Lucchetta[19-21] also proved that increased melt temperature and holding pressure result in increased bonding strength in PP-based TCM. Their results showed that bonding strength decreases with increasing mold temperature. Interestingly, Macedo et al.[22] found that holding pressure is the main processing parameter that governs the bonding strength between PP-g-MA and an overmolded PA6 layer.

Simulations in process design require a strong mathematical background for each phenomenon that occurs during the studied process. On the one hand, injection molding is a well-known field for simulation[23-25], and several CAE packages are available for modeling injection molding. On the other hand, the simulation of the bonding strength between the substrate and overmolded elements is missing in all available simulation software.

The theoretical background of the fusion bonding of thermoplastics can be found in the literature. It involves two phenomena: intimate contact and healing. During overmolding, molten material is injected or deposited on a substrate under pressure; this ensures intimate contact. Healing (or autohesion) is the interdiffusion of polymer molecules across the bonding interface. Healing commences when the temperature rises above the glass transition temperature (T_g) in amorphous thermoplastics or the melt temperature (T_m) in semi-crystalline thermoplastics. Le Maoult et al.[26] proved that the temperature of the interface between fused glass fiber reinforced polycarbonate (PC) and PC filled with carbon black should be well above the T_g of PC for good cohesion and perfect chain entanglement.

The theory that describes the healing process of thermoplastics was introduced by de Gennes in the 1970s[27]. It is called "reptation theory." The reptation model represents the location and movement of macromolecules in amorphous polymers[28]. Macromolecules (with a chain length of L) are considered to be surrounded by a tube, which is a steric border between them and other molecules. When the temperature of a polymer rises above a certain level (T_g or T_m), the molecule chain starts to leave the tube. First, the end of the molecule chain (l), called the "minor chain", escapes from the tube. Then more and more of the chain leaves the tube. The time in which the whole molecule chain escapes from the tube ($l = L$), is called reptation time (Figure 2). To some extent, reptation time characterizes the transition of a polymer chain from one equilibrium state into another. Wool et al.[13] reported that relaxation time, which is derived from viscosity measurements, can be used as reptation time.

The reptation model was successfully used in evaluating bonding strength in the following cases: weld lines during injection molding[29], the welding of polymer films[30], the fusion bonding of polymers[31], and bonding between the layers of TPC

manufactured by Automated Fiber Placement (AFP) and Automated Tape Placement (ATP) process[32].

Researchers have proposed several analytical models to describe the bonding between two thermoplastic components. All these models use the degree of healing (D_h):

$$D_h = \frac{\sigma}{\sigma_\infty},$$

where σ is the actual bonding strength, and σ_∞ is the strength of a single-piece part.

Bastien and Gillespie were the first to propose two mathematical models for bonding strength for the non-isothermal fusion bonding of amorphous polymers. In the first model (hereafter "Model 1"), they derived the expression of the degree of healing starting from the incremental growth of the minor chain length (Eq. 1):

$$D_h = \frac{\sigma}{\sigma_\infty} = \left(\frac{l}{L}\right)^{1/2} = \left[\sum_{i=0}^{n} \frac{t_{i+1}^{1/2} - t_i^{1/2}}{t_{rep}(T)^{1/2}}\right]^{1/2}, \quad (1)$$

In their second model (hereafter "Model 2"), they started from the bonding strength increment (Eq. 2). The experimental results in their study demonstrated that Model 2 was more accurate [32]:

$$D_h = \frac{\sigma}{\sigma_\infty} = \sum_{i=0}^{n} \frac{t_{i+1}^{1/4} - t_i^{1/4}}{t_{rep}(T)^{1/4}}, \quad (2)$$

where t_i is the time in the current time step, and t_{rep} is the reptation time at the current temperature T.

Sonmez and Hahn proposed a mathematical model in an integral form to describe non-isothermal healing (hereafter "Model 3", Eq. 3) [33]:

$$D_h = \frac{\sigma}{\sigma_\infty} = \left[\int_o^t \frac{d\tau}{2\sqrt{\tau \cdot t_{rep}(\tau)}}\right]^{1/2}, \qquad (3)$$

where τ is the time interval.

However, later Yang and Pitchumani[34] proved that Model 1, Model 2, and Model 3 adequately describes the behavior of polymers only under isothermal conditions. Moreover, the above-mentioned models are only valid for low molecular weight polymers—traditional engineering thermoplastics typically have a high molecular weight (M_w). Yang and Pitchumani stated that materials with a high M_w need less time than the reptation time to achieve maximum bonding strength. They formulated a model (hereafter "Model 4") that describes the non-isothermal healing of high M_w amorphous thermoplastics:

$$D_h = \frac{\sigma}{\sigma_\infty} = \left[\int_o^t \frac{1}{t_w(T)} dt\right]^{1/4}, \qquad (4)$$

where t_w is the welding time (Figure 2).

There are several mathematical models in the literature for the calculation of the bonding strength between two amorphous thermoplastics. However, processing simulation software packages do not contain any of these models. Therefore, they cannot predict bonding strength for injection overmolding. Another problem is that none of the above-mentioned analytical models considers the unique parameters and boundary conditions of overmolding. The models assume that the temperature is the same on the whole interface. However, during overmolding, the temperature distribution on the interface is uneven. Moreover, the temperature of the base plate and that of the overmolded part are also different. Several studies [21, 25] proposed a method that combines diffusion theory with the 1D temperature field simulation to assess adhesion at the welding interface. However, none of them provides a relationship

between the processing parameters and bonding strength. The above-mentioned studies do not consider the unevenness of the temperature distribution at the interface, either. The latest study of Akkerman et al.[35] combined an analytical model of the degree of healing with the Moldflow simulation software, taking into account the unevenness of the temperature distribution on the interface. However, this study focused on semi-crystalline polymers, which require completely different analytical models to describe healing. The authors did not calculate strength, only the degree of healing.

Therefore, the goal of our study is to create a method that predicts the bonding strength between the high M_w amorphous polymer substrate and the overmolded element using the above-mentioned mathematical models. Our model considers the uneven temperature distribution along and across the bonding surface as well. The modeling results will be verified with experiments. Our novel method can also be incorporated into existing injection molding simulation software.

Materials and methods

Materials

Three different amorphous polymers were used in the tests (Table 1). We did the main part of the research with ABS (Styrolution Terluran GP35), and the control experiments with PC (Makrolon 2805) and PS (Versalis Edistir n3910). All the materials were dried according to their requirements (Table 1).

Testing

Processing conditions and test samples

We designed a new geometry for the test specimen, a so-called “rib-on-plate geometry” (Figure 3), to characterize the overmolding process. This test specimen consists of an

80 mm × 80 mm × 2 mm base plate, which we manufactured separately by conventional injection molding with a melt temperature of 260 °C and a mold temperature of 60 °C. The other part of the test specimen is a 70 mm × 63 mm × 2 mm overmolded rib produced by direct injection. After removing the sprue from the part, we investigated the interface that formed between the two components.

For manufacturing the overmolded elements, we developed a mold (Figure 4), which is equipped with a mechanically operated slider to accommodate the base plate. This mold can be used without the base plate; hence we can also produce single-piece specimens with it. This way, the base plate and the rib can be injection molded as one single part for reference. We mounted two pressure sensors (Cavity eye, RC15) and three IR temperature sensors (Futaba EPSSZL-4x30) into the mold. These sensors provided important data about the process and helped us set switchover.

Mechanical testing

For the tensile tests, we used a Zwick Z020 universal tensile testing machine (Zwick Roell AG, Germany). For the rib-on-plate test specimen, we developed a grip (Figure 4)[9]. The upper holder plate of the grip has a 3 mm wide slot in the middle, where we placed the rib of the specimen. The rib was clamped with the conventional grip at the bottom. Testing speed was 5 mm/min, and we tested 5 specimens for each set of processing parameter combination.

Rheological characterization

We ran a frequency sweep test on the samples using a parallel plate rotational rheometer (AR2000, TA Instruments) to find the angular frequency at which *G'* equals *G"*. The relaxation time of the material for each temperature was measured in different frequency ranges (**Hiba! A hivatkozási forrás nem található.**). The shear strain

applied was 0.5 %, the diameter of the plates was 25 mm, and their thickness was 1.2 mm. These samples were manufactured on an Arburg Allrounder 270S (ARBURG GmbH) injection molding machine.

Overmolding processing parameters

The average cycle time for overmolding was slightly above 50 seconds. Before injection, the base plate was kept in the closed mold for 20 seconds. This ensured that the temperature of the base plate reached T_{mold}, which was either 40 °C or 80 °C. We produced sample parts at different melt temperatures: 220 °C, 240 °C, 260 °C, 280 °C, and 300 °C. We set up a flow rate of 40 cm^3/s for the injection phase. The switchover position was controlled through an internal pressure transducer placed close to the end of the cavity. We used 75 MPa for 2 seconds for the holding phase. The parts were ejected after a residual cooling time of 22 seconds. The parts were kept at room temperature for 6 hours before the tensile tests.

Numerical modeling of overmolding

The temperature of the interface is necessary for the calculation of bonding strength. To the best of our knowledge, none of the studies considered the 2D temperature distribution in the interface. All the studies focused on the 1D temperature distribution in the interface of the coupled materials [20, 21]. The novelty of the current study is that it combines analytical and numerical approaches to estimate bonding strength and consider the spatial and temporal unevenness of temperature distribution in the interface. We obtained the temperature field history from the simulation in Moldflow (Moldflow Insight 2019, Autodesk Inc.) and created a 3D model of the specimen and the simplified mold with the cooling channels (Figure 5).

We used tetrahedral elements to mesh the model. The average mesh size was 1.2 mm for the components of the specimen, while we reduced the mesh element size to 0.3 mm in the contact surface area and the surrounding area to increase the accuracy of the simulation.

For the mold, we used a structured mesh. On the area where the part is in contact with the mold, we used the same mesh size as for the part, while further away from this region, a larger mesh element size was used. In the regions with the cooling channels, the mesh was smoother to make the calculation of heat transfer more accurate. The mesh for the mold and the cooling channels contained 2.7 million elements, while the part had 2.5 million elements. For the contact surface, we used a precise mesh—there were 4750 nodes on the base plate and the same amount of identically positioned nodes on the rib.

We ran the simulations with the same process parameters as the parameters used during manufacturing. For example, the initial mold temperature was set to 40 °C or 80 °C. To model cooling, we used a transient cooling mode, in which the mold temperature changes during the cycles. To compensate for part ejection time and the time required to insert the base plate, we set 5 seconds for “open mold time” in the simulation. After 5 seconds, the mold closed, and the base plate was kept in the mold for 20 seconds before injection started. This way, the base plate reached the temperature of the mold. The injection molding sequence was set as close to the real-life sequence as possible. The flow rate for the injection phase was 40 cm^3/s, followed by the holding phase with 75 MPa for 2 seconds. The time for filling, holding, and cooling together was set to 25 seconds. The simulation yielded the temperature distribution along the interface as a function of time on both the base plate and the rib (Figure 6).

In the case of injection overmolding, the temperature history of the interface is different for each node. Therefore, we exported the temperature history data for each node from the simulation results (Figure 7).

Results and discussion

The calculation of temperature history

The original models of bonding strength (Eq. 1-4) assume that the two components and the whole contact surface have the same temperature. However, during overmolding, the two surfaces have slightly different temperatures due to the imperfect heat transfer between the components. Besides that, the temperature distribution is uneven along the interface. Due to these reasons, the current models (Eq. 1-4) cannot accurately predict the bonding strength of the interface between the substrate and the overmolded rib.

The interface was modeled as described earlier, thus we have coincident nodes on the base plate and the rib. The temperature histories of the coincident nodes are different. Therefore, we determined the average temperature of those pairs of nodes and named them $T_{node}(t)$. Only those regions are used for the calculations where both temperatures are above T_g (Figure 8). When the overmolded polymer melt meets with the base plate, it has a maximum temperature and then starts to cool down rapidly until it reaches a temperature close to the average temperature of the interface. By contrast, the temperature of the base plate starts to increase until it reaches a temperature close to the average temperature of the interface.

The calculation of bonding strength

The reptation time at given temperatures is needed for the calculation of bonding strength. As discussed in the Introduction, it can be assumed that the reptation time is

equal to the relaxation time of the polymer at a given temperature. The relaxation time at a specific temperature is the time after which the elastic modulus (*G'*) of the polymer is equal to its storage modulus (*G"*). We obtained the relaxation time of ABS GP-35 at different temperatures from the viscosity curves. We ran a frequency sweep test on the samples using a parallel plate rotational rheometer (AR2000, TA Instruments) to find the angular frequency at which *G'* equals *G"* (Figure 9). At the reference temperature of 170 °C, the coefficient of variation of the repeated tests did not exceed 4%—we repeated each test five times (Figure 9).

Above the glass transition temperature, the reptation time was determined as a function of temperature; the reptation time is necessary for the calculation of bonding strength. We fitted the Williams-Landel-Ferry (WLF) equation (Eq. 5) to the measured reptation time values to obtain a continuous function (Figure 10).

$$\log a_T = log \frac{t_{rep}}{t_{rep}(T_{ref})} \qquad (5)$$

where a_T is the shift factor, t_{rep} is the reptation time at temperature T, T_{ref} is the reference temperature, and C_1 and C_2 are constants. 210 °C was used as the reference temperature because it was in the middle of the tested range. For this temperature, the calculated reptation time was 0.4635 s.

As mentioned before, the reptation time is infinite if the temperature is lower than T_g. The graph of the WLF equation has a discontinuity with a vertical asymptote, which depends on C_2:

$$\lim_{T \to T_{ref} - C_2} \left(\frac{t_{rep}}{t_{rep}(T_{ref})} \right) \to \infty$$

The WLF equation has a discontinuity, whose position depends on C_2. At this point, the value of the function is infinite:

$$t_{rep}(T) = \infty, \qquad if\ T = T_r - C_2$$

With the previous equations, C_2 is equal to:

$$C_2 = T_r - T_g = 210\ °C - 103\ °C = 107\ °C$$

We calculated the other constant, C_1, at every measured point, then averaged those values:

$$C_1 = 2.23$$

The reptation time (Figure 11) was calculated for every pair of nodes from $T_{node}(t)$ with the WLF equation. For any given moment, if $T_{node}(t)$ is below T_g, diffusion will not take place at the given pair of nodes, and local bonding strength will not increase between them.

With the reptation time curves, we determined the degree of healing with the four mathematical models that are currently available in the literature. Model 1 and Model 2 operate with discrete time intervals for the reptation time, while Model 3 and Model 4 use continuous functions for the calculations.

With all four analytical models, the degree of healing (D_h) can be calculated at all nodes separately. The degree of healing shows the ratio between the evolved and the maximum bonding strength that can be achieved; thus, D_h has to be between 0 and 1 ($0 \leq D_h \leq 1$). To compare the modeling and experimental results, we determined D_h for the whole contact surface with the equations from the literature for each process parameter set, e.g. different mold and melt temperatures. The calculations with all the four models were as follows:

(1) D_h^i was determined for each pair of nodes (where *i* is the number of the pair of nodes in the mesh),

(2) we calculated the average overall D_h^{av} for the whole contact surface by averaging the individual D_h^i values.

We determined the minimum and maximum theoretical borders for the degree of healing (D_h^{min}, D_h^{max}) by simply choosing the minimum and maximum values from D_h^i, unless there were any nodes under T_g in the entire cycle because then it changes D_h^{min} to zero (Figure 12).

Mesh distribution affects the accuracy of the calculation of D_h^{av}. Since an even mesh distribution was used, the calculation was precise with the above-mentioned method.

From the four different models, we chose Model 4 to present the D_h results (Figure 10). Bonding strength was calculated (Eq. 6) with all four models and their accuracy was compared to the measured strength.

$$\sigma_{calc} = \sigma_\infty \cdot D_h^{av}, \qquad (6)$$

where σ_{calc} is the calculated bonding strength, σ_∞ is the maximum bonding strength (the tensile strength of single-piece specimens, and D_h^{av} is the average degree of healing calculated with the selected model.

Experimental results and modeling

The base plates were manufactured separately by conventional injection molding. Melt temperature was 260 °C, and mold temperature was 60 °C. In the overmolding phase, the temperature of the melt was 220 °C, 240 °C, 260 °C, 280 °C, and 300 °C, while mold temperature was 40 °C and 80 °C. Bonding strength was tested with ten samples

for each set of parameters. We manufactured single-piece specimens with all the different mold and melt temperatures. The tensile strength in each case was almost the same. The average tensile strength (33.7 MPa) was used as maximum bonding strength (σ_∞).

After we calculated bonding strength (Eq. 5) with each model (Eq. 1-4), we verified these results with the measured bonding strengths (Figure 13).

Bonding strength values yielded by three out of the four analytical models are in good agreement with the measured bonding strengths. Model 1 produced the best correlation with the experimental data, with an error of 7 %. Models 3 and 4 gave similar results with an error of 11.0 % and 11.2 %, respectively. Model 2 exhibited worse results with the largest error of more than 200 %, which is the opposite of Bastien and Gillespie's results [31].

We found that bonding strength increases with melt temperature and mold temperature. Bonding strength is a saturation curve as a function of melt temperature. With different mold temperatures, these curves are shifted. Thus, different segments of a saturation curve can be seen in Figure 13.

We tried our calculation method on other amorphous polymers (PC and PS) as well. In both cases, melt temperature was chosen based on the material datasheet of the polymer. We used Model 4 for our calculation. The results are in good agreement with the measured bonding strength (Figure 14). The good agreement between the simulation and experimental results proves the validity of the proposed simulation method and proves that our calculation method can be used for a range of amorphous polymers in cases where bonding process is temperature-dependent. Therefore, this calculation method justifies its implementation in numerical simulation software. However, the proposed simulation method still requires some modifications to improve its accuracy.

Conclusions

We developed an original calculation method to predict the bonding strength between a base plate and an overmolded element. The novelty of the method is a combination of analytical and numerical approaches to estimate bonding strength and consider the spatial and temporal unevenness of temperature distribution in the interface. We simulated the overmolding process to obtain the temperature history of the contact surface and used four mathematical models to calculate the degree of healing. The modeling results were verified through the mechanical testing of injection overmolded samples. We verified the simulation results with two different mold temperatures and five different melt temperatures. The results obtained with the proposed simulation method are in good agreement with the test results. We proved that our simulation-based method predicts the bonding strength of overmolded elements with an error of 7%.

In the case of ABS, the maximum bonding strength between an overmolded element and a substrate is 25 MPa, while the theoretical maximum of bonding strength is 33.7 MPa. We found that the bonding strength of overmolded specimens increased with melt temperature and mold temperature.

Funding. This work was supported by the National Research, Development and Innovation Office, Hungary (2019-1.1.1-PIACI-KFI-2019-00205, 2018-1.3.1-VKE-2018-00001, 2017-2.3.7-TÉT-IN-2017-00049). The research reported in this paper was supported by the BME NC TKP2020 grant of NKFIH Hungary.

Acknowledgments. We wish to thank ARBURG HUNGÁRIA KFT. for the ARBURG Allrounder 370S 700-290 injection molding machine, TOOL-TEMP HUNGÁRIA KFT., LENZKES GMBH and PIOVAN HUNGARY KFT. for the accessories. The researchers are grateful to Moldex3D for their technical support.

References

[1] Bhambure, D.D.; Yadav, S.D. A review on advance composite material for automotive body application. Int. Res. J. of Eng. and Tech. 2020, 7 (2), 2926-2930.

[2] Schmitt, M. Additive manufacturing infill optimization for automotive 3d-printed abs components. Rap. Protot. J. 2020, 26, 89-99. DOI: 10.1108/RPJ-01-2019-0007

[3] Reddy, K.S.; Dufera, S. Additive Manufacturing Technologies. Int. J. of Man., Inf., Tech. and Eng. 2016, 4 (7), 89-112.

[4] Ageyeva, T.; Sibikin, I.; Karger-Kocsis, J. Polymers and related composites via anionic ring-opening polymerization of lactams: Recent developments and future trends. Pol. 2018, 10. DOI: 10.3390/polym10040357

[5] Sibikin, I.; Karger-Kocsis, J. Toward industrial use of anionically activated lactam polymers: Past, present and future. Adv. Ind. and Eng. Pol. Res. 2018, 1, 48-60. DOI: 10.1016/j.aiepr.2018.06.003

[6] Herzog, J.; Wendel, R.; Weidler, P.G.; Wilhelm, M.; Rosenberg, P.; Henning, F. Moisture adsorption and desorption behavior of raw materials for the T-RTM process. J. of Comp. Sci. 2021, 5 (1), 12. DOI: 10.3390/jcs5010012

[7] Sherman, L.M. The new lightweights: Injection molded 'hybrid' composites spur auto innovation. https://www.ptonline.com/articles/the-new-lightweights-injection-molded-hybrid-composites-spur-automotive-innovation (accessed 21 January 2020).

[8] Gardiner, G. Camisma's car seat back: Hybrid composite for high volume. https://www.compositesworld.com/articles/camismas-car-seat-back-hybrid-composite-for-high-volume (accessed 21 January 2020).

[9] Boros, R.; Rajamani, P.K.; Kovács, J.G. Combination of 3d printing and injection molding: Overmolding and overprinting. eXPRESS Pol. Let. 2019, 13, 889–897. DOI: 10.3144/expresspolymlett.2019.77

[10] Hürkamp, A.; Gellrich, S.; Ossowski, T.; Beucher, J.; Thiede, S.; Herrmann, C.; Dröder, K. Combining Simulation and Machine Learning as Digital Twin for the Manufacturing of Overmolded Thermoplastic Composites. Manuf. and Mat. Proc. 2020, 4 (3), 92. DOI: 10.3390/jmmp4030092

[11] Yang, F.; Pitchumani, R. Nonisothermal healing and interlaminar bond strength evolution during thermoplastic matrix composites processing. Pol. Comp. 2003, 24, 263-278. DOI: 10.1002/pc.10027

[12] Stokes-Griffin, C.M.; Compston, P. An inverse model for optimisation of laser heat flux distributions in an automated laser tape placement process for carbon-fibre/peek. Comp. Part A: Appl. Sci. and Manuf. 2016, 88, 190-197. DOI: 10.1016/j.compositesa.2016.05.034

[13] Wool, B.R.; Tuan, B.-L.; Mcgarel, O.J. Welding of polymer interfaces. Pol. Eng. and Sci. 1989, 29, 1340-1367.

[14] Schell, J.S.U.; Guilleminot, J.; Binetruy, C.; Krawczak, P. Computational and experimental analysis of fusion bonding in thermoplastic composites: Influence of process parameters. J. of Mat. Proc. Tech. 2009, 209, 5211-5219. DOI: 10.1016/j.jmatprotec.2009.03.008

[15] Wolf, M.; Hertle, S.; Drummer, D. Influence of the thermomechanical properties on the joining of adhesion incompatible polymers by form-fit using the vibration welding process. eXPRESS Pol. Let. 2019, 13, 365–378. DOI: 10.3144/expresspolymlett.2019.30

[16] Fiberform lightweight parts. The perfect combination of thermoforming and injection molding. KraussMaffei, Ed. Germany, p 11.

[17] Holmes, M. Composite technologies to the fore at k. Reinf. Plast. 2020, 64 (5), 261-267. DOI: 10.1016/j.repl.2019.12.088

[18] Candal, M.V.; Gordillo, A.; Perez, O.S.; Sanchez, J.J. Study of the adhesion strength on overmoulded plastic materials using the essential work of interfacial fracture (ewif) concept. J. of Mat. Sci. 2008, 43, 5052-5060. DOI: 10.1007/s10853-008-2667-1

[19] Giusti, R.; Lucchetta, G. Modeling the adhesion bonding mechanism in overmolding hybrid structural parts for lightweight applications. Key Eng. Mat. 2014, 611-612, 915-921.

[20] Giusti, R.; Lucchetta, G. Analysis of the welding strength in hybrid polypropylene composites as a function of the forming and overmolding parameters. Pol. Eng. and Sci. 2017, 58, 592-600. DOI: 10.1002/pen.24786

[21] Giusti, R.; Lucchetta, J. Modeling the adhesion bonding strength in injection overmolding of polypropylene parts. Pol. 2020, 12 (9), 2063. DOI: 10.3390/polym12092063

[22] Macedo, S.; Lafrance, E.; Martins, C.I.; Douchain, C.; Loux, C.; Krawczak, P. Thin wall injection-overmolding of polyamide 6/polypropylene multilayer parts: PA6/PP-g-MA interfacial adhesion investigations.Appl. Pol. Sci. 2020, 138, 17. DOI: 10.1002/app.50294

[23] Wang, M.-L.; Chang, R.-Y.; Hsu, C.-H. 5 - molding simulation methodology. In: Wang M-L, Chang R-Y, Hsu C-H, editors. Molding simulation: Theory and practice; Hanser: Munich; 2018; pp. 123-158. DOI: 10.3139/9781569906200.005pp 123-158.

[24] Wang, M.-W.; Arifin, F.; Vu, V.-H. The study of optimal molding of a LED lens with grey relational analysis and molding simulation. Periodica Polyt. Mech. Eng. 2019, 63, 278-294. DOI: 10.3311/PPme.13337.

[25] Benayad, A.; El Otmani, R.; El Hakimi, A.; Boutaous, M.; Touache, A.; Musa, R.K.; Derdouri, S.; Mahfoudi, N.; Siginer, D. Experimental investigation and numerical simulation of the microinjection molding process through an expanding flow configuration. Pol. Adv. Tech. 2021, N/a, 1-22. DOI: 10.1002/pat.5206.

[26] Akue Asseko, A.C.; Cosson, B.; Lafranche, E.; Schmidt, F., Le Maoult, Y. Effect of the developed temperature field on the molecular interdiffusion at the interface in infrared welding of polycarbonate composites. Comp. Part B. 2016, 97, 53-61. DOI: 10.1016/j.compositesb.2016.04.064

[27] de Gennes, P.G. Reptation of a polymer chain in the presence of fixed obstacles. J. Chem. Phys. 1971, 55, 572. DOI: 10.1063/1.1675789

[28] Eslami, H.; Grmela, M. Mesoscopic formulation of reptation. Rheol. Acta. 2008, 47, 399-415. DOI: 10.1007/s00397-007-0239-y.

[29] Cruz, C.A. Integrative simulation for assessing the mechanical performance of a weld line on injection moulded thermoplastic parts. In Proceedings of 11th World Congress on Computational Mechanics (WCCM XI), 5th European Conference on Computational Mechanics (ECCM V) and 6th European Conference on Computational Fluid Dynamics (ECFD VI), Barcelona, Spain, 20-24 July, 2014.

[30] Grewell, D.; Benatar, A. Semi-empirical, squeeze flow and intermolecular diffusion model. I. Determination of model parameters. Pol. Eng. & Sci. 2008, 48, 860-867. DOI: 10.1002/pen.21021

[31] Bastien, L.J.; Gillespie Jr., J.W. A non-isothermal healing model for strength and toughness of fusion bonded joints of amorphous thermoplastics. Pol. Eng. & Sci. 1991, 31, 1720-1730. DOI: 10.1002/pen.760312406

[32] Yassin, K.; Hojjati, M. Processing of thermoplastic matrix composites through automated fiber placement and tape laying methods: A review. J. of Thermopl. Comp. Mat. 2017, 31, 1676-1725. DOI: 10.1177/0892705717738305

[33] Sonmez, F.O.; Hahn, H.T. Analysis of the on-line consolidation process in thermoplastic composite tape placement. J. of Thermopl. Comp. Mat. 1997, 10, 543-572.

[34] Yang, F.; Pitchumani, R. Healing of thermoplastic polymers at an interface under nonisothermal conditions. Macromol. 2002, 35, 3213-3224. DOI: 10.1021/ma010858o

[35] Akkerman, R.; Bouwman, M.; Wijskamp, S. Analysis of the thermoplastic composite overmolding process: interface strength. Frontier in Mat. 2020, 7, 16. DOI: 10.3389/fmats.2020.0002

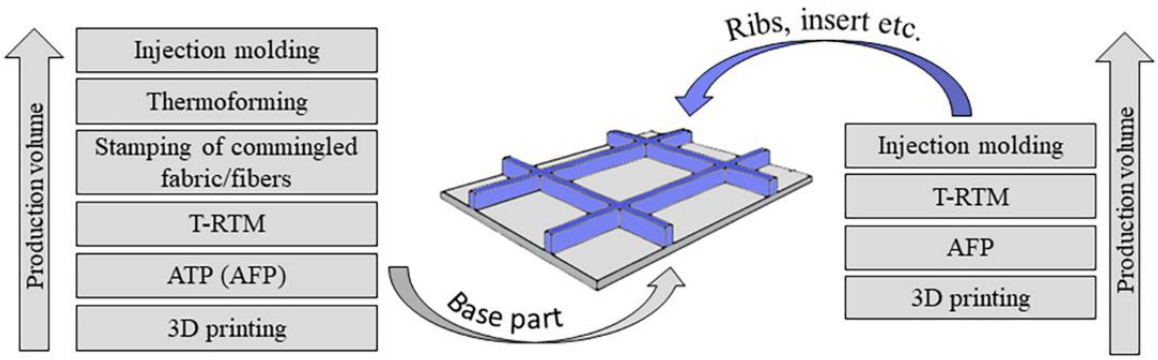

Figure 1. Conceptual scheme of a hybrid TCM process (AFP – automated fiber placement)

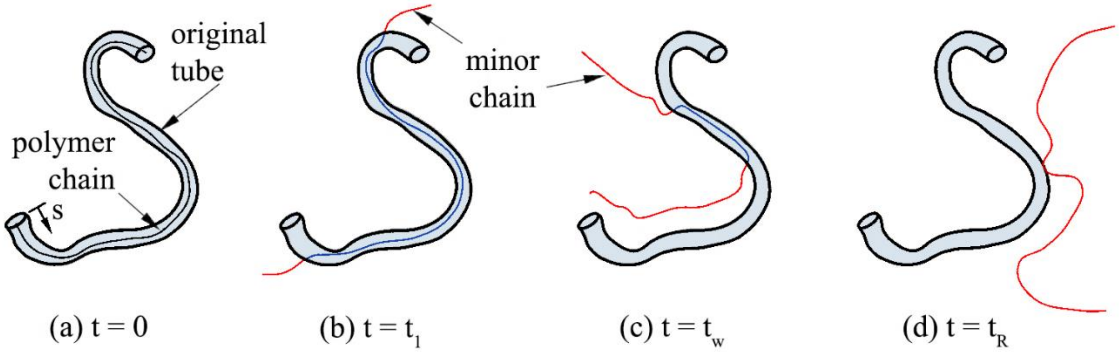

Figure 2. Reptation movement of a linear polymer chain, and reptation time, in which the whole chain escapes from the original tube [9]

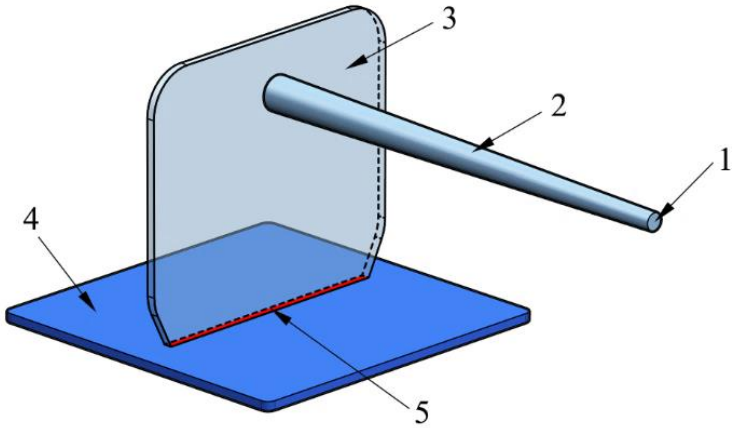

Figure 3. Rib-on-plate test specimen: 1 – injection point, 2 – sprue, 3 – rib (component 2), 4 – base plate (component 1), 5 – interface (contact surface)

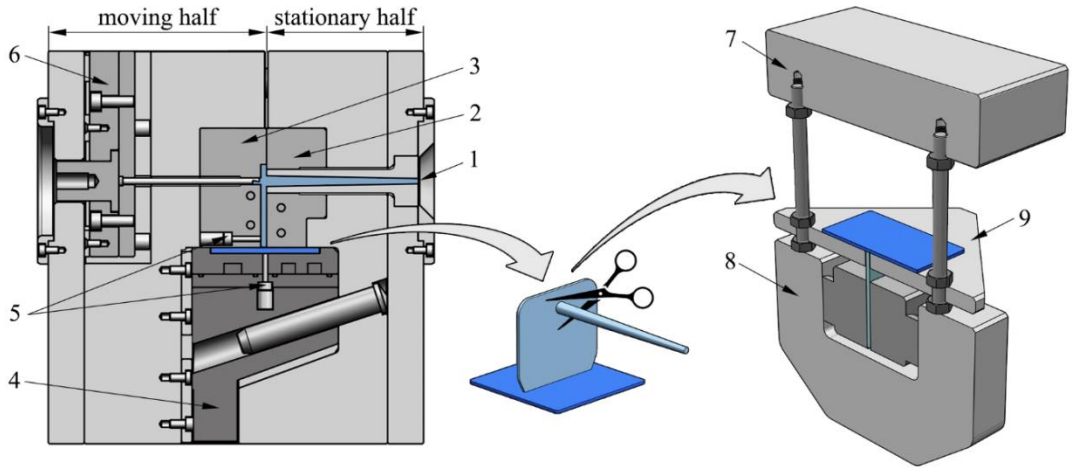

Figure 4. Overmolding mold and tensile test setup: 1 – injection point, 2 – cavity insert, 3 – core insert, 4 – slider, 5 – pressure and IR temperature sensors, 6 – ejection system, 7 – tensile machine, 8 – vise, 9 – gripper plate

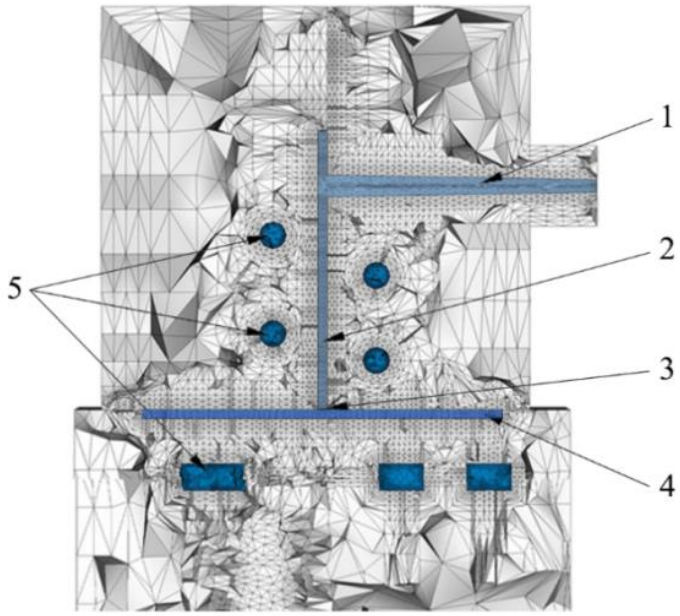

Figure 5. 3D tetrahedral finite element mesh of the mold (the grey areas are the parts of the mold and inserts): 1 – sprue, 2 – rib, 3 – interface (contact surface), 4 – base plate, 5 – cooling channels

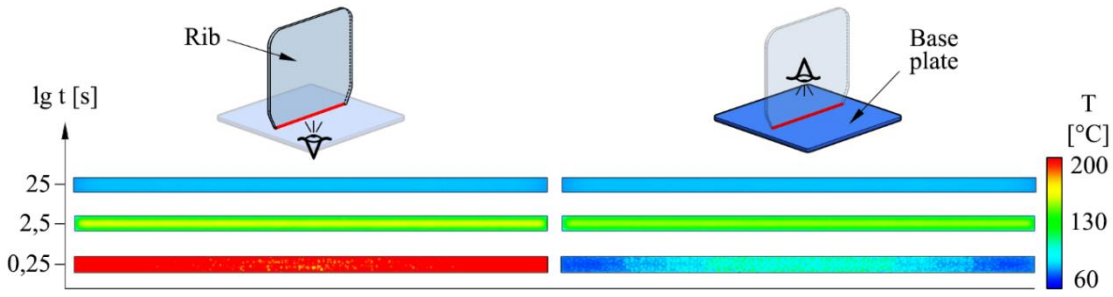

Figure 6. Temperature distributions at different times on the contact surfaces on the rib and the base plate side

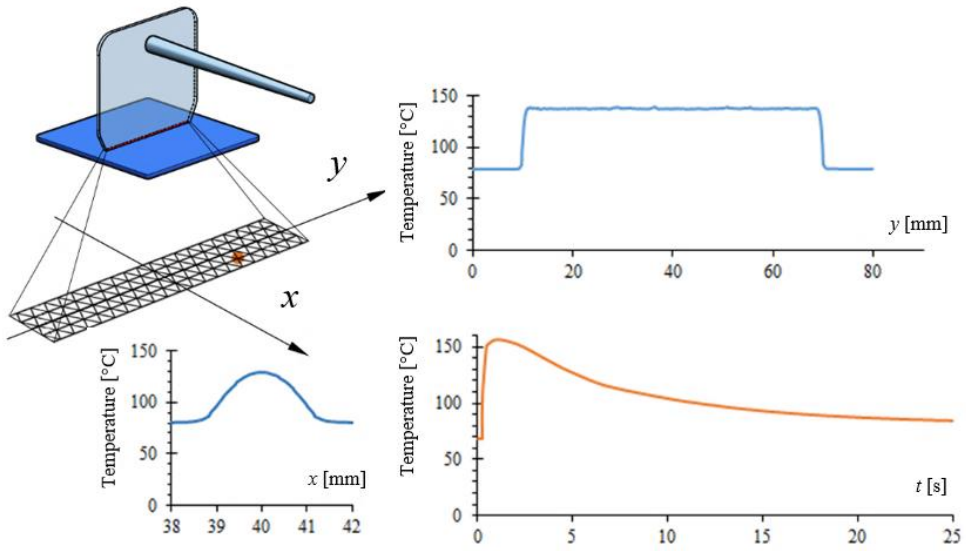

Figure 7. The components and the interface with the nodes ($T_n(t)$ – the temperature of an arbitrary node as a function of time, $T(x,y)$ – the temperature distribution along a certain cross-section at a particular moment)

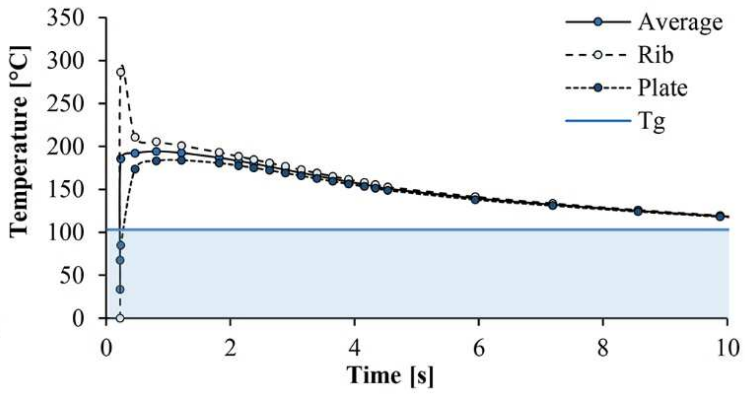

Figure 8. The typical temperature history of one pair of nodes on the rib/plate interface

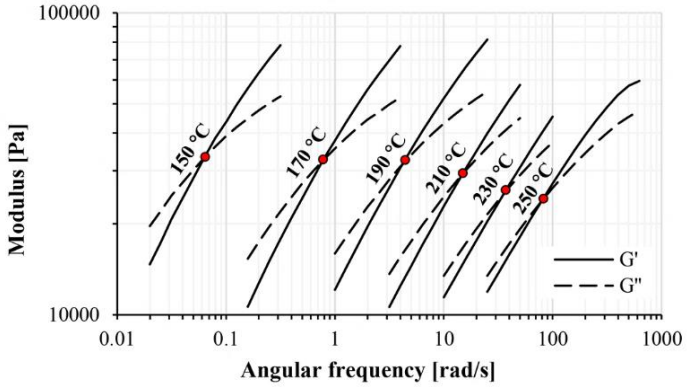

Figure 9. The frequency sweep test to obtain relaxation time

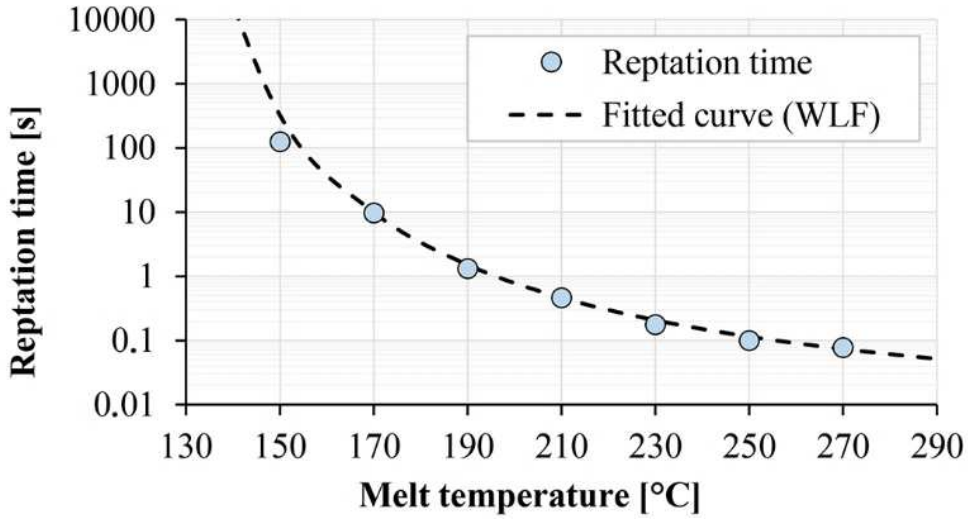

Figure 10. The temperature dependence of reptation time with the fitted WLF curve

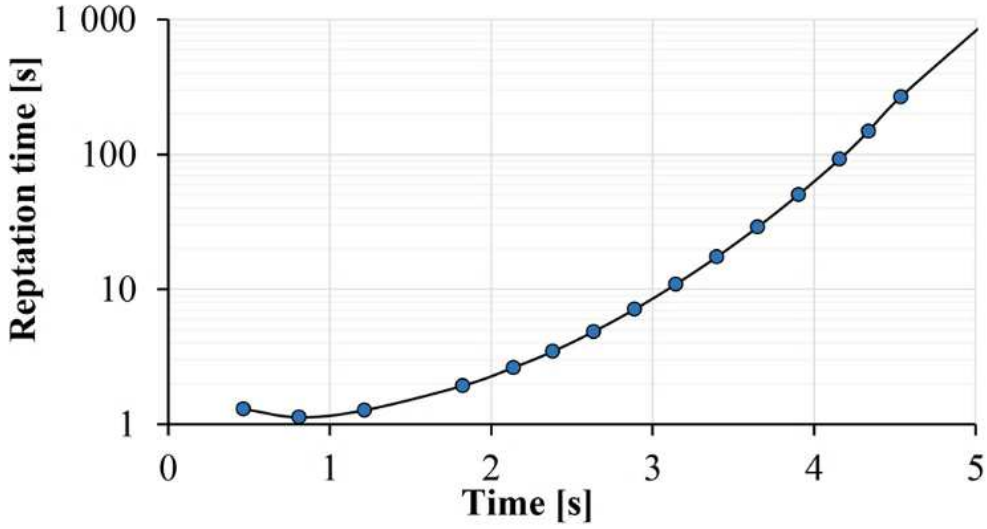

Figure 11. The reptation time as a function of time for an individual pair of nodes

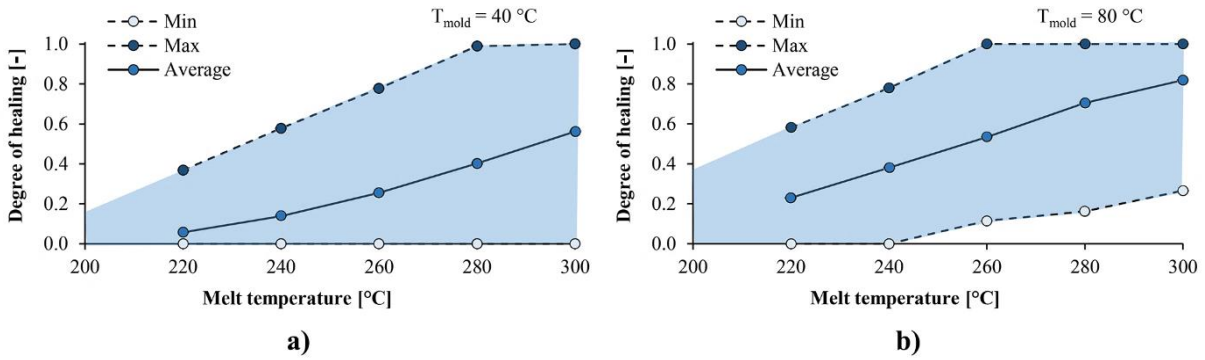

Figure 12. The minimum, maximum and average degree of healing calculated with Yang's model at a mold temperature of a) 40 °C and b) 80 °C as a function of melt temperature.

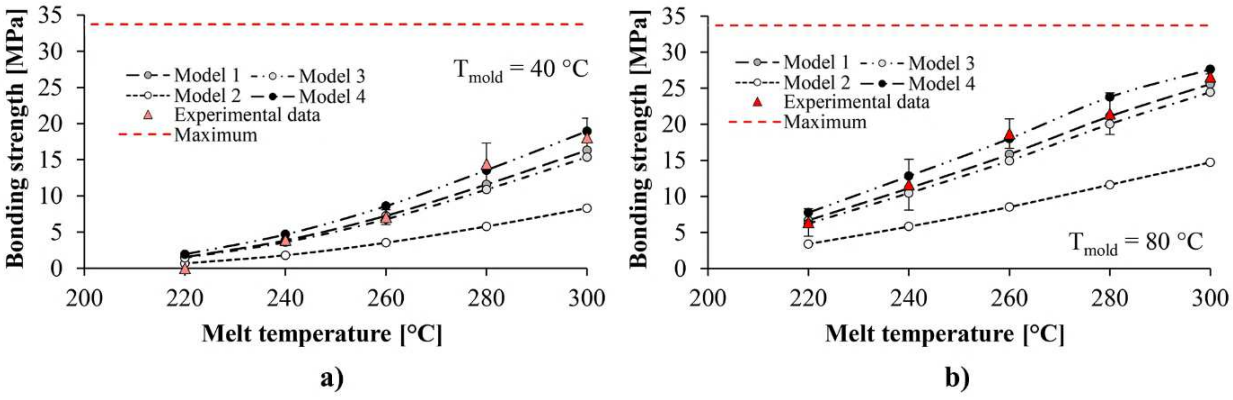

Figure 13. Experimental and calculated overall bonding strength with a mold temperature of a) 40 °C and b) 80 °C. Maximum stands for the strength of the single-piece specimens and Experimental data are the measured bonding strengths

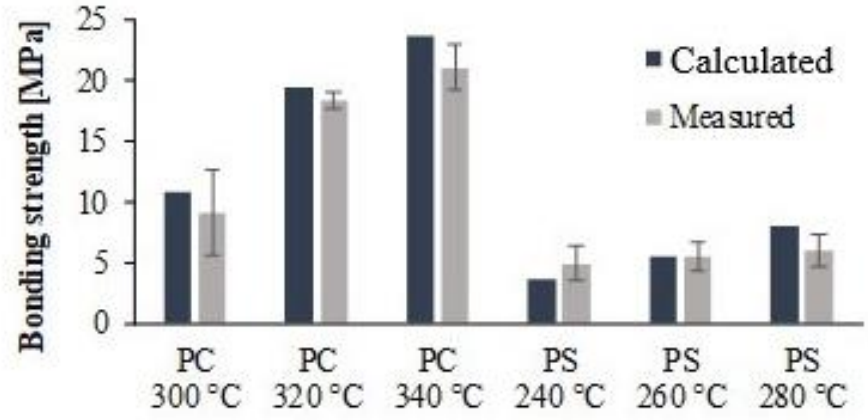

Figure 14. Experimental and calculated overall bonding strength with PC and PS

Table 1. Properties of the examined materials

Material	Styrolution Terluran GP-35 ABS	Convestro Makrolon 2805 PC	Versalis Edistir n3910 PS
Drying temperature and time	80 °C for 4 hours	120 °C for 4 hours	Not required
Recommended melt temperature range	220–280 °C	280–320 C	200–250 °C
Mold temperature	40 °C and 80 °C	80 °C	30 °C

Table 2. Test temperatures and the corresponding frequency ranges

Temperature [°C]	Frequency range [rad/s]
130	0.01 – 1
150	0.01 – 100
170	0.1 – 100
190	0.1 – 100
210	1 – 100
230	1 – 100
250	1 – 628.3
270	1 – 628.3
290	10 – 628.3
310	10 – 628.3